



Received 00th January 20xx,
Accepted 00th January 20xx

DOI: 10.1039/x0xx00000x

www.rsc.org/

Solution-processable, Niobium-doped Titanium Oxide Nanorods for Application in Low-voltage, Large-area Electronic Devices

F. A. Alharthi,^{a,c} F. Cheng,^a E. Verrelli,^b N. T. Kemp,^b A. F. Lee,^d M. A. Isaacs,^e M. O'Neill^b and S. M. Kelly*^a

We report for the first time the one-step synthesis of solution-processable, highly crystalline, niobium-doped titanium dioxide (Nb-TiO₂) nanorods in the anatase phase by the hydrolytic condensation of Ti(OⁱPr)₄ and niobium (V) ethoxide using oleic acid as a structure-directing and stabilising agent. These novel surface-stabilised nanorods can be easily dispersed in common solvents at relatively high concentration (~10%) and deposited as uniform, thin and transparent films on planar substrates for the fabrication of electronic devices. The small size of the nanoparticles synthesized represents an important advance in achieving high-*k* dielectric thin films smooth enough to be suitable for OFET applications and the plastic electronics field in general. Preliminary investigations show that the dielectric constant, *k*, of niobium-doped (7.1 wt%) titanium dioxide (Nb-TiO₂) nanorods at frequencies in the region of 100 kHz-1 MHz, are more a third greater (*k* > 8) than that (*k* = 6) determined for the corresponding undoped titanium dioxide (TiO₂) nanorods. The current-voltage (*J*-*V*) behaviour of these devices reveal that niobium-doping improves, by reducing, the leakage current of these devices, thereby preventing hard dielectric breakdown of devices incorporating these new nanorods.

Introduction

Solution-processable and printable electronics is forecast to become a major disruptive technology, not by replacing conventional electronic devices, but by opening new markets based on flexible, low-weight and mechanically robust substrates and low-cost, deposition-from-solution manufacturing processes, such as roll-to-roll fabrication of displays, transistors, photovoltaics, RFID tags, etc. The sequential processing of different material classes, such as organic semiconductors, metal oxide semiconductors or dielectrics, conducting polymers or metallic colloids, to form multi-layered uniform thin films, is often required to realise such devices.¹⁻³ Although the colossal dielectric permittivity of

niobium-doped titanium-dioxide ceramics have been reported,^{4,5} these were prepared by solid state synthesis requiring sintering temperatures up to 1400 °C and hence are unsuited to electronic film fabrication processes and to plastic electronic applications.

Solution-processable high-dielectric constant, *k*, materials are highly sought after as an inexpensive route to plastic electronic devices, and have the potential to replace silicon dioxide as a gate dielectric to enable further miniaturisation of electronic components. Polymers doped with nanoparticles to create high-*k* polymer composites represent a potentially attractive approach to create high-*k* gate dielectrics from solution for plastic electronics. However, major challenges of this approach, still to be resolved, include the realization of stable, homogeneous nanoparticle dispersions as well as the tailoring of stable polymer/nanoparticle interfaces required to achieve the desirable electrical performance.⁶⁻⁸

Titanium dioxide is a very promising material for application in hybrid organic/inorganic photovoltaic device applications due to the high dielectric constants of the anatase (*k* = 31) and rutile (*k* = ~114) phases.^{9,10} Resistive switching has also been demonstrated in titanium dioxide thin films designed for application in next-generation, non-volatile memory devices.¹¹ In order to render titanium dioxide nanoparticles soluble - and therefore processable - from organic solution, their surface

^a School of Mathematics and Physical Sciences, Chemistry, University of Hull, Cottingham Road, Hull, HU6 7RX, United Kingdom.

^b School of Mathematics and Physical Sciences, Physics, University of Hull, Cottingham Road, Hull, HU6 7RX, United Kingdom.

^c Department of Chemistry, College of Science, King Saud University, P.O. Box 2455, Riyadh 11451, Kingdom of Saudi Arabia.

^d Department of Chemistry, University of York, York, YO10 5DD, United Kingdom.

^e European Bioenergy Research Institute, Aston University, Birmingham B4 7ET, United Kingdom

† Footnotes relating to the title and/or authors should appear here.

Electronic Supplementary Information (ESI) available: [details of any supplementary information available should be included here]. See DOI: 10.1039/x0xx00000x

must first be functionalised with organic ligands/surfactants in order to overcome the strong inter-nanoparticle adhesion forces.¹² Ligands with long, flexible aliphatic chains are often used to stabilise spherical or rod-shaped inorganic nanoparticles and thereby inhibit their aggregation/sintering.¹³ Such hybrid organic/inorganic nanocomposites do not suffer from phase separation over time, since a uniform monolayer of the organic coating is chemically bound to the surface of the nanoparticles. The ability to synthesise short, surface-stabilised, semiconductor nanorods, soluble in common solvents used to deposit semiconductor materials on plastic electronic substrates using spin coating, drop casting, inkjet printing, Doctor blade and related techniques, etc., with a low degree of dispersity, also facilitates the formation of uniform, thin dielectric layers with the desired dielectric and other electrical, electronic and physical properties.

One-dimensional (1D) nanostructures such as nanorods, nanowires, nanobelts and nonotubes, have attracted much attention for optoelectronic applications and photocatalysis due to their anisotropic features, high aspect ratios and high surface-area-to-volume ratios, which offer a high density of sites available for surface reactions, better load-transfer in composites, and higher (interfacial) charge-carrier transfer rates.¹⁴ Hydrothermal and solvothermal processing, templating, electrospinning and solution-phase reactions have been developed to prepare such titanium dioxide nanorods.^{15–17} The non-hydrolytic synthesis of titanium dioxide nanorods with high crystallinity and organic surface coatings has attracted considerable recent interest in relation to the fabrication of solution-processed plastic electronic devices.¹⁸ Weller et al. reported a one-step, low-temperature method to prepare well-crystallized oleic acid-capped, titanium dioxide nanorods in the anatase phase by hydrolysis of titanium tetraisopropoxide [Ti(OⁱPr)₄], using oleic acid as the surfactant and tertiary amines or quaternary ammonium hydroxides as catalysts.¹⁹ Concentrated colloidal dispersions in organic solvents can be easily prepared from such oleic acid-capped titanium dioxide nanorods. Oleic acid-capped titanium dioxide nanorods have also been prepared from Ti(OⁱPr)₄ at higher reaction temperatures of 260–270 °C.²⁰ Shaffer et al reported the preparation of solution-processable anatase titanium dioxide nanorods by two-step non-hydrolytic condensation reactions between TiCl₄ and Ti(OⁱPr)₄ in the presence of oleic acid.¹⁸ Recently, niobium-doped titanium dioxide (Nb-TiO₂) nanorods (Nb = 3 wt%) have been prepared by low-temperature (120 °C) hydrolytic condensation of NbCl₅ and Ti(OⁱPr)₄ in the presence of oleic acid, **but the nanorods were not homogenous.**²¹

Nanoscale niobium-doped titanium-dioxide particles (Nb-TiO₂) have attracted increasing attention due to their electronic properties and potential applications.^{22–24} Lu et al showed that optical transparency and electrical conductivity of the niobium-doped titanium-dioxide (Nb-TiO₂) thin films prepared by reactive, remote-plasma sputtering deposition are comparable to those for tin-doped indium oxide (Sn-TiO₂ or ITO), offering significant potential for the low-carbon processing of niobium-doped titanium-dioxide layers (Nb-TiO₂) as a substitute for ITO

as standard industry electrodes and hole-injecting layers that require scarce and expensive indium.²⁵

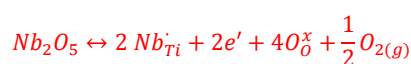
Kim et al have successfully used niobium-doped anatase titanium-dioxide nanoparticles as photoanodes in organic dye-sensitized solar cells (DSSCs),²⁶ while Duta et al showed that niobium-doped titanium-dioxide multilayer films (1–10 layers) in the anatase phase are suitable for environmental carbon monoxide sensors.²⁷ Yu et al reported that niobium-doped titanium-dioxide rod electrodes exhibit enhanced electrical conductivity, high reversible capacity, long cycle life and excellent rates capability, and hence can be employed as an anode material in lithium-ion batteries.²⁸ More recently, niobium- and indium-doped titanium-dioxide (Nb-In-TiO₂) ceramics were shown to be high-potential dielectric materials.^{4,5,29} Niobium-doped titanium-dioxide ceramics (Nb_xTi_{1-x}O₂, where x = 1–8 atom%) with giant permittivity (>104) and a very low dielectric loss (~0.05) were prepared by sintering rutile TiO₂ and Nb₂O₅ mixed powders under flowing N₂ at 1400 °C for 10 h.⁴ The electron-pinned defect-dipoles were confirmed as the origin of both their high permittivity and low dielectric loss in the high frequency range for resulting Nb_xTi_{1-x}O₂ ceramics with x > 4 atom%. Mandal et al also reported the enhancement of the dielectric constant of sintered titanium dioxide films upon doping with niobium.⁵ High-density rutile Ti_{1-x}Nb_xO₂ (x = 0.0, 0.02, 0.04, 0.06 and 0.1) was prepared from a mixture of TiO₂ and Nb₂O₅ by sintering at 1400 °C for 48 h. The heterogeneous microstructure consisting of semiconducting grains and insulating grain boundaries was reported to unlock micro-capacitors with high permittivity (~104 at room temperature and 1 kHz). In addition, intrinsic defect dipoles also contributed towards the high permittivity.

Niobium is an excellent foreign atom for isostructural incorporation into the TiO₂ lattice because its ionic radii $r(\text{Nb}^{5+}) = 0.064 \text{ nm}$ is close to that of Ti^{4+} ($r(\text{Ti}^{4+}) = 0.0605 \text{ nm}$).³⁰ Since Nb⁵⁺ has one additional valence electron compared to Ti⁴⁺, the charge compensation of Nb⁵⁺ in substitution to Ti⁴⁺ comes from either by the creation of Ti cation vacancy, or by the stoichiometric reduction of Ti⁴⁺ to Ti³⁺, depending upon the ambient oxygen activity. Under oxidizing conditions, incorporated Nb is compensated ionically by titanium vacancies as showing in the following chemical equilibria:



$$[\text{Nb}_{\text{Ti}}^{\cdot}] = 4[V_{\text{Ti}}^{\prime\prime\prime}]$$

Under reducing conditions, Nb incorporation involves electronic compensation by electrons as showing in the following chemical equilibria:³¹



$$[\text{Nb}_{\text{Ti}}^{\cdot}] = n$$

Here, we report the *ex-situ* synthesis of solution-processable, highly crystalline niobium-doped titanium dioxide (OA-Nb-TiO₂) nanorods by hydrolytic condensation of Ti(OⁱPr)₄

and niobium (V) ethoxide [Nb(OEt)₅, NBE0] or niobium isopropoxide [Nb(OⁱPr)₅, NBIO], using oleic acid as a surfactant and surface stabiliser in combination with tertiary amines or quaternary ammonium hydroxides as reaction catalysts. The electrical properties of these oleic-acid-stabilised, niobium-doped titanium dioxide (OA-Nb-TiO₂) nanorods were expected to be superior to those of the corresponding non-doped oleic-acid-stabilised, titanium dioxide (OA-TiO₂) nanorods, which exhibit high solubility in common organic solvents used to deposit thin, smooth, and transparent films of the solute on device substrates for low-cost, plastic electronic applications using standard processes, such as spin coating, drop casting, inkjet printing, Doctor blade techniques, etc.,¹⁹ but low values for the dielectric constant, *k*, and high leakage currents in standard crossbar test devices.

Experimental

Synthesis of Oleic acid-stabilized, niobium-doped titanium oxide nanorods (OA-Nb-TiO₂)

$Ti(OR)_4 + xR'CO_2H \rightarrow Ti(OR)_{4-x}(R'CO_2)_x + xROH$	(1)
$Nb(OR)_5 + xR'CO_2H \rightarrow Nb(OR)_{5-x}(R'CO_2)_x + xROH$ $R = -CH(CH_3)_2, -CH_2CH_3, R' = -C_{17}H_{33}$	(2)
$(OR)_{3-x}(R'CO_2)_xTi(OR) + (R'CO_2)Ti(OR)_{4-x}(R'CO_2)_{x-1}$ $\rightarrow (OR)_{3-x}(R'CO_2)_xTi - O$ $- Ti(OR)_{4-x}(R'CO_2)_{x-1} + R'CO_2R$	(3)
$(OR)_{4-x}(R'CO_2)_xNb(OR) + (R'CO_2)Nb(OR)_{5-x}(R'CO_2)_{x-1}$ $\rightarrow (OR)_{4-x}(R'CO_2)_xNb - O$ $- Nb(OR)_{5-x}(R'CO_2)_{x-1} + R'CO_2R$	(4)
$(OR)_{3-x}(R'CO_2)_xTi(OR) + (R'CO_2)Nb(OR)_{5-x}(R'CO_2)_{x-1}$ $\rightarrow (OR)_{3-x}(R'CO_2)_xTi - O$ $- Nb(OR)_{5-x}(R'CO_2)_{x-1} + R'CO_2R$	(5)
$(OR)_{4-x}(R'CO_2)_xNb(OR) + (R'CO_2)Ti(OR)_{4-x}(R'CO_2)_{x-1}$ $\rightarrow (OR)_{4-x}(R'CO_2)_xNb - O$ $- Ti(OR)_{4-x}(R'CO_2)_{x-1} + R'CO_2R$	(6)
$ROH + R'CO_2H \rightarrow R'CO_2R + H_2O$	(7)
$Ti(OR)_{4-x}(R'CO_2)_x + yH_2O \rightarrow Ti(OR)_{4-x-y}(R'CO_2)_x + yROH$	(8)
$Nb(OR)_{5-x}(R'CO_2)_x + yH_2O$ $\rightarrow Nb(OR)_{5-x-y}(R'CO_2)_x + yROH$	(9)

The oleic acid-stabilized, niobium-doped titanium oxide (OA-Nb-TiO₂) nanorods were prepared by co-hydrolysis of titanium (IV) tetraisopropoxide (TTIP) and niobium precursors, niobium isopropoxide (NBIO) and niobium (V) ethoxide (NBE0), using oleic acid as solvent and surfactant at low temperature (100 °C). Trimethylamine *N*-oxide (TMAO) was added as a catalyst for the polycondensation in order to form a crystalline product in a similar way to titanium alkoxides, which readily react with carboxylic acids in mild conditions to form titanium oxocarboxyalkoxide, see equation 1.¹⁹ Niobium oxocarboxyalkoxides are also formed when niobium alkoxides were added in oleic acid at 85 °C, see equation 2. Ti-O-Ti, Nb-O-Nb and Ti-O-Nb networks formed by non-hydrolytic condensation and/or elimination of an ester, see equations 3-6.¹⁹ Hydrolysis, see equation 8 and 9, also occurred after a slow

esterification, see equation 1. The hydrolysis products may continue the non-hydrolytic condensation, see equations 3-6 to further generate Ti-O-Ti, Nb-O-Nb and Ti-O-Nb networks.

Titanium (IV) tetra-isopropoxide (TTIP, ≥97.0 %), oleic acid (90 %), trimethylamine *N*-oxide (TMAO, 98 %) and niobium (V) ethoxide (NBE0, 99.95%) were sourced from Sigma-Aldrich. Niobium isopropoxide (NBIO, 99%) was sourced from Alfa Aesar. Ultrapure water with a specific resistance of 18.2 MΩ·cm was obtained by reversed osmosis followed by ion-exchange and filtration (UPQ PS system, ELGA, USA). **Pure N₂ gas cylinder was provided by Energas Ltd, UK**

Chemical and physical characterisation

Fourier transform infrared spectra were recorded on a Nicolet Magna-500 FTIR spectrometer. Transmission electron microscopy (TEM) was collected using a Jeol 2010 TEM running at 200kV. Images were obtained with a Gatan Ultrascan 4000 digital camera. The liquid sample was mixed well in a vial, a 5μL aliquot is placed on a hydrophilic carbon coated copper grid and allowed to air dry. X-ray powder diffraction (XRD) analyses were performed on a PAN analytical Empyrean Series 2 Diffractometer. The concentration of the titanium and barium present in the samples was determined on the Perkin Elmer Optima 5300DV emission ICP instrument. The concentration of carbon, hydrogen and nitrogen present in the samples was analysed by Fisons EA 1108 CHN apparatus. Polarized optical microscopy (POM) was conducted on an Olympus BH2 polarising microscope, with images taken by polarizers in a perpendicular arrangement. X-ray photoelectron spectroscopy (XPS) was undertaken on a Kratos Axis HSi spectrometer fitted with a charge neutralizer and magnetic focusing lens, employing Al K_α monochromatic radiation (1486.7 eV). Spectral fitting was performed using CasaXPS version 2.3.14. Binding energies were corrected to the C 1s peak at 284.6 eV and surface atomic compositions calculated *via* correction for the appropriate instrument response factors.

Dielectric characterisation

The electrical properties of oleic-acid-stabilised, niobium-doped (7.12% and 5.6%) titanium dioxide (OA-Nb-TiO₂) nanorods **S4** and **S5**, respectively, and that of the corresponding non-doped, oleic-acid-stabilised, titanium dioxide (OA-TiO₂) nanorods, for comparison purposes, were tested using a crossbar approach. A crossbar device consists of a sandwich of the test material between two metallic electrodes perpendicular to each other, i.e., the bottom and top electrodes. Glass slides cut to size and cleaned using acetone and propan-2-ol were used as substrates. The bottom and top electrodes were made of aluminium, deposited using an E306 Edwards thermal evaporator, and the patterns were created via using a custom made self aligning shadow mask set. The materials were deposited on the bottom electrode patterns via solution processing and spin coating. Solutions of concentrations 10 wt% in chlorobenzene were used and spincoating was carried out in static mode at 1000 rpm for 30 s followed by a 10 min bake at 100 °C. The film thickness was kept in the range 270-320 nm. Due to the small size of the nanoparticles used, the surface of these thin films is relatively

flat, characterised by a surface roughness of 2-3 nm RMS and good uniformity over large areas with maximum peak-valley height difference of ~ 25 nm over a $1 \mu\text{m}^2$. Electrical characterisation measurements were carried out in inert environment using a custom built triaxial probe station system equipped with a Solartron 1260 impedance analyser and an Agilent B2912 source measure unit. The dielectric constant of the materials was extracted from the parallel capacitance resulting from analysing the impedance data using a simple R-C (resistance-capacitance) parallel model for our test cross-bar devices.

Experimental details for the synthesis of oleic-acid-stabilised, niobium-doped titanium oxide (OA-Nb-TiO₂) nanorods S1-S6

Oleic acid (420 g) was dried under vacuum for 1 h at 120 °C and then allowed to cool to 85 °C. Titanium (IV) isopropoxide (17.7 cm³, 60 mmol) was added under nitrogen to form a clear yellow solution. After stirring for 10 minutes, the required amount of niobium precursors was injected quickly to the yellow solution, see table 1. Then, a solution of trimethylamine *N*-oxide (2 M, 60 cm³) was added rapidly by syringe to the reaction mixture. The reaction temperature was then increased to 100 °C and the reaction mixture allowed to react for either a further 24 h or 72 h, see table 1. After cooling to room temperature, isopropanol (1.2 L) was added to the reaction mixture and the resultant precipitate was separated off by centrifugation, washed twice with isopropanol and then dried overnight under vacuum at 30 °C. This solid product was suspended in toluene and then precipitated from this solution by adding acetone before being separated off by centrifugation. This purification step was repeated twice and the resultant solid product dried overnight under vacuum at 30 °C to give the desired oleic acid-stabilised, niobium-doped titanium dioxide (OA-Nb-TiO₂) nanorods S1-S6, see table 1.

Results and discussion

Physical properties

The effect of the niobium precursors on the oleic-acid-stabilised, niobium-doped titanium oxide (OA-Nb-TiO₂) nanorods S1-S6, see Table 1, can be observed from the products prepared after 72 h reaction. Analysis by ICP indicates that the molar ratio of Ti:Nb in the products S1 and S2 prepared using niobium isopropoxide (NBIO) as a reaction precursor was 74.5:1 and 77.8:1, respectively, which were much higher than those (9:1 and 19:1, respectively) for the starting materials (TTiP:NBIO), see Table 1. However, the molar ratio of Ti/Nb in the products S4 and S6 prepared using niobium ethoxide (NBEO) as a reaction precursor was 10.2:1 and 18.3:1, respectively, values which are close to those (9:1 and 19:1, respectively) for the starting reagents (TTiP:NBEO), see Table 1. One possible reason is for these differences would be that

niobium oxocarboxyethoxide may have a similar non-hydrolytic condensation speed as that of titanium oxocarboxyisopropoxide, which results in products with a similar Ti:Nb ratio to that of the starting materials TTiP:NBEO. As for NBIO, the higher Ti:Nb ratio comparing with the starting materials TTiP:NBIO ratio is probably due to the slower non-hydrolytic condensation speed of niobium oxocarboxyisopropoxide compared to that of titanium oxocarboxyisopropoxide.

Table 1 also shows the effect of reaction time on the composition of the oleic acid-stabilised and niobium-doped titanium dioxide (OA-Nb-TiO₂) nanorods S1-S6. It can be seen that the molar ratio of Ti:Nb in the product S5 prepared during a 24 h reaction is 13.7:1, much lower than that (19.0:1) of the TTiP:NBEO starting materials. At higher reaction times (72 h), the molar ratio of Ti:Nb in S6 is 18.3:1, which is very close to that (19.0:1) of the TTiP:NBEO starting materials. This difference is possibly due to the fact that some of titanium oxocarboxyisopropoxide may not have completely converted to oleic acid-capped titanium oxide in the 24 h reaction, which is supported to some degree by the low product yield for this reaction, i.e., 1.47 g for S6 compared to 1.20 g for S5.

The XRD patterns of the oleic-acid-stabilised, niobium-doped titanium dioxide (OA-Nb-TiO₂) nanorods S1 and S3-S6 and those of the corresponding non-doped oleic-acid-stabilised, titanium dioxide (OA-TiO₂) nanorods shown in Figure 1 (a-e and f, respectively) are very similar.¹⁹ Only peaks attributable to titanium dioxide in the anatase state are observed, with no Nb₂O₅ or NbO₂, for the oleic-acid-stabilised, niobium-doped titanium dioxide (OA-Nb-TiO₂) nanorods S1 and S3-S6. **These findings suggest that niobium may have been incorporated into the titanium dioxide lattice,^{32,33} or Nb₂O₅ or NbO₂ may be present in the amorphous form.**

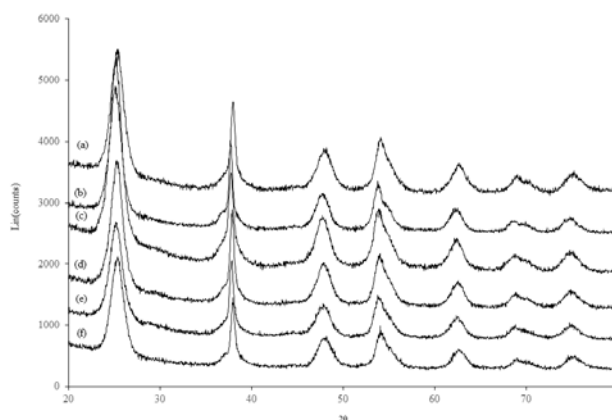
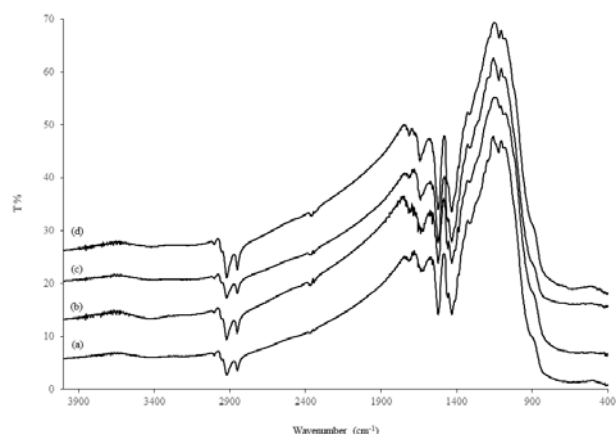


Figure 1 XRD patterns (a-e) of the oleic-acid-stabilised, niobium-doped titanium dioxide (OA-Nb-TiO₂) nanorods S1 and S3-S6 and (f) non-doped oleic acid-stabilised titanium dioxide (OA-TiO₂) nanorods

Table 1 Reaction conditions and chemical analysis of the oleic acid-stabilised and niobium-doped titanium dioxide nanorods **S1-S6**.

Sample	Nb precursor [*]	Ti/Nb (reaction)	Time (h)	Yield (g)	Ti ^a (%)	C ^b (%)	H ^b (%)	N ^b (%)	Nb ^a (%)	Ti/Nb (product)
S1	NBIO	9:1	72	1.50	41.1	19.14	3.05	0.34	1.07	74.5:1
S2	NBIO	19:1	72	1.47	44.1	21.24	3.30	0.49	1.10	77.8:1
S3	NBEO	9:1	24	1.65	39.2	18.78	3.00	0.63	8.02	9.5:1
S4	NBEO	9:1	72	1.75	37.5	19.05	2.97	0.67	7.12	10.2:1
S5	NBEO	19:1	24	1.20	39.5	18.87	2.94	0.53	5.60	13.7:1
S6	NBEO	19:1	72	1.47	39.7	21.20	3.35	0.60	4.20	18.3:1

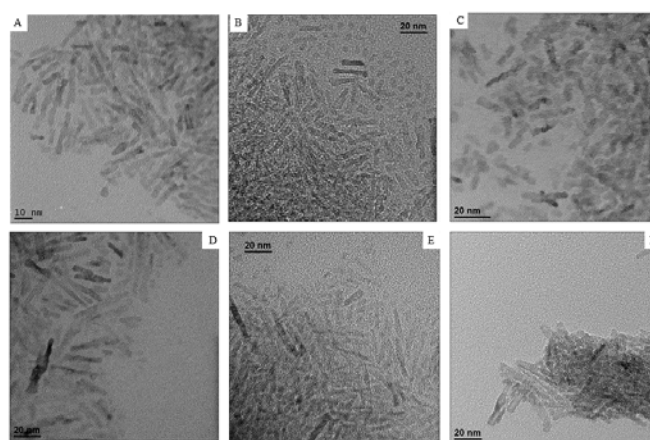
^{*}NBIO = Niobium isopropoxide; NBEO = Niobium (V) ethoxide. ^aICP, ^bCHNS

**Figure 2:** FT-IR patterns of the oleic acid-stabilised, niobium-doped titanium dioxide nanorods (TiO₂-OA-Nb) (a) **S3**, (b) **S4**, (c) **S5** and (d) **S6**.

The FT-IR spectra of the oleic acid-stabilised, niobium-doped titanium dioxide (OA-Nb-TiO₂) nanorods **S3-S6**, prepared from NBEO, are shown in Figure 2. The IR absorption peaks observed at 2850, 2920 and 2955 cm⁻¹, attributable to C-H₃, C-H₂ and C-H the oleic acid coating with titanium centres of the surface of the nanorods.^{34,35} In addition, the stretch vibrations, are indicative of the presence of (organic) oleic acid bound to the surface these (inorganic) nanorods. The two strong peaks at 1525 and 1430 cm⁻¹, a frequency difference around $\Delta\nu_{a-s} = 95$ cm⁻¹, are attributable to asymmetric and symmetric stretching vibrations of the bidentate carboxy (COO⁻) group, indicating the interaction of carboxyl groups present in the oleic acid coating with titanium centres of the surface of the nanorods.^{34,35} In addition, the very weak and broad stretch at 3465 cm⁻¹ indicates

the presence of trace hydroxyls on the surface of the nanorods. The presence of oleic acid on the surface of the nanorods is also supported by elemental analysis, which indicates the presence of both carbon and hydrogen at relatively high concentrations, i.e., 20 % and 3 %, respectively, see Table 1.

Analysis of HRTEM images show that the shape and aspect ratios (5 to 8) of the oleic acid-stabilised, niobium-doped titanium dioxide (OA-Nb-TiO₂) nanorods **S1-S6**, see Figure 3(b-f), are very similar to those of the corresponding non-doped oleic acid-stabilised, titanium dioxide (OA-TiO₂) nanorods, see Figure 3(a), which strongly suggests that the presence of a relatively high concentration of niobium in the former nanorods has very little impact on their shape or size, which again is consistent with the incorporation of all of the niobium in the reaction mixture into the titanium dioxide lattice.

titanium dioxide nanorods (OA-TiO₂) and the oleic acid-stabilised,

niobium-doped titanium dioxide nanorods (OA-Nb-TiO₂) (b) **S1**, (c) **S3**, (d) **S4**, (e) **S5** and (f) **S6**.

The surface composition and chemical environment of the oleic-acid-stabilised, niobium-doped titanium dioxide (OA-Nb-TiO₂) nanorods **S4-S6**, prepared from NBEO, were investigated using XPS, see Figures 4 and 5 for high-resolution Nb 3d and Ti 2p XP, respectively. The Ti 2p XP spectra for non-doped oleic-acid-stabilised, titanium dioxide (OA-TiO₂) nanorods are also shown in Figure 5 for the purposes of comparison. The surface concentrations and binding energies of Ti(III,IV) and Nb(IV,V) chemical states derived from XPS peak fitting are summarised in Table 2. The Nb 3d XP spectra exhibit the characteristic Nb 3d doublet with 3d_{5/2} and 3d_{3/2} spin-orbit components at 207.0 eV and 209.6 eV, respectively (Figure 4). Peak fitting reveals principally Nb⁵⁺ at 207.0 eV³⁶ and a small contribution from Nb⁴⁺ around 205.9 eV.^{37,38} The Nb⁴⁺/Nb⁵⁺ ratios for **S3-S6** are shown in Table 2 and span 0.13-0.08. We therefore conclude that Nb⁵⁺ is the principal dopant within the TiO₂ matrix, co-existing with trace Nb⁴⁺. Figure 5 shows that the analogous non-doped oleic-acid-stabilised, titanium dioxide (OA-TiO₂) nanorods has 2p_{3/2} and 2p_{1/2} 2p binding energies of 458.45 eV and 464.10 eV,

respectively, similar to those observed for all the oleic-acid-stabilised, niobium-doped titanium dioxide (OA- and 2.7% respectively) is higher than that (2.03%) determined for the corresponding non-doped oleic-acid-stabilised, titanium dioxide (OA-TiO₂) nanorods associated with a small number of oxygen vacancies arising from equations 11 and 12.⁴ It is well known that the introduction of Nb⁵⁺ into TiO₂ can increase the Ti³⁺ content due to charge compensation, as shown in equations 10 and 12.^{4,40} However, the concentration of Ti³⁺ determined for **S3-S6** is significantly lower than the amount of Nb introduced (10 atom% for **S3** and **S4** and 5 atom% for **S5** and **S6**). This observation has been previously reported for ceramics doped with high Nb levels (>4 atom%).⁴ It was reported that higher Nb level will provide excessive electrons, which can be captured by oxygen vacancies in Eq. 11 to further transform into O_o. Equation 11 will reduce the concentration of electrons, which in turn will limit the extent of Ti⁴⁺ reduction in Equation 12 and hence the Ti³⁺ concentration.⁴ The 2(Nb⁵⁺)[•]_{Ti} → 4(Ti³⁺)[•]_{Ti} ← V_O^{••} defect complex, in which electrons and oxygen vacancies are located in the limited lattices, will lead to the formation of electron-pinned defect dipoles.⁴

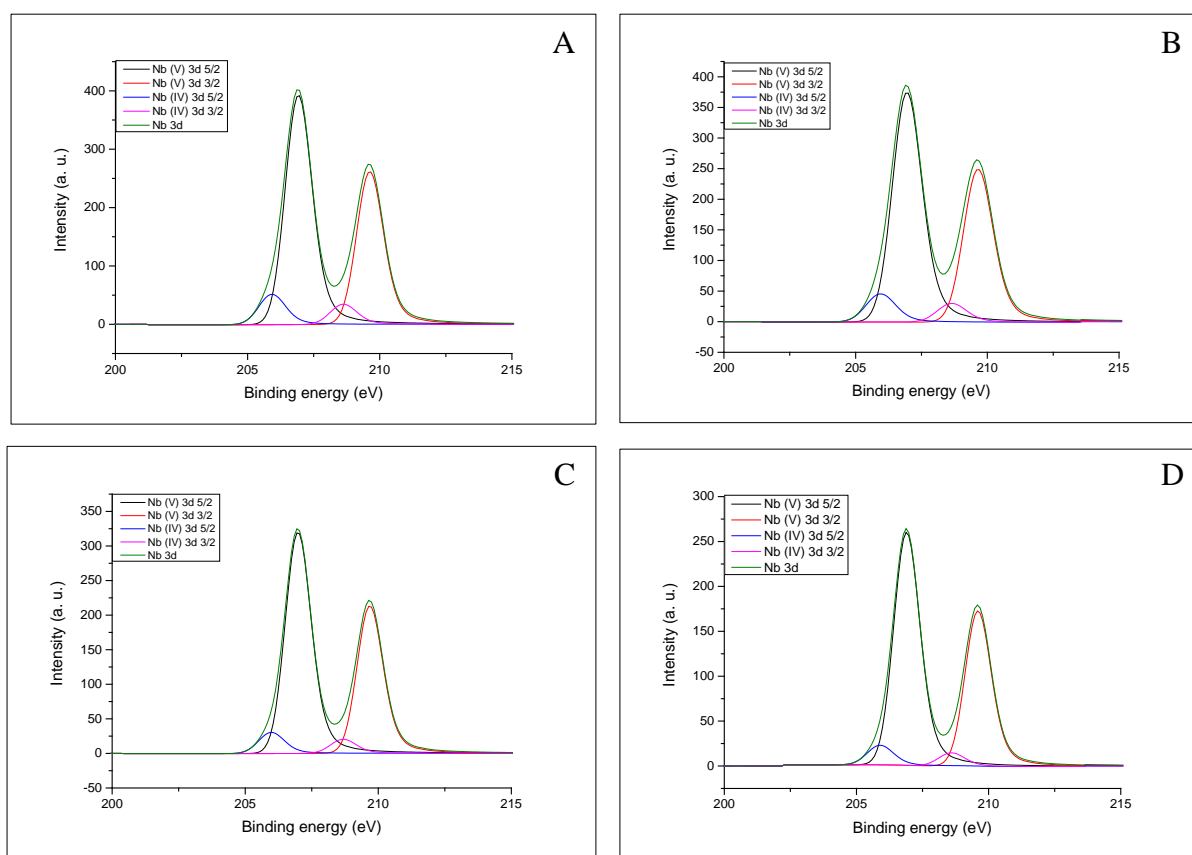


Figure 4 Nb 3d XP spectra of the oleic-acid stabilised, niobium-doped titanium dioxide nanorods (TiO₂-OA-Nb), prepared from NBEO, (A) **S3**, (B) **S4**, (C) **S5** and (D) **S6**.

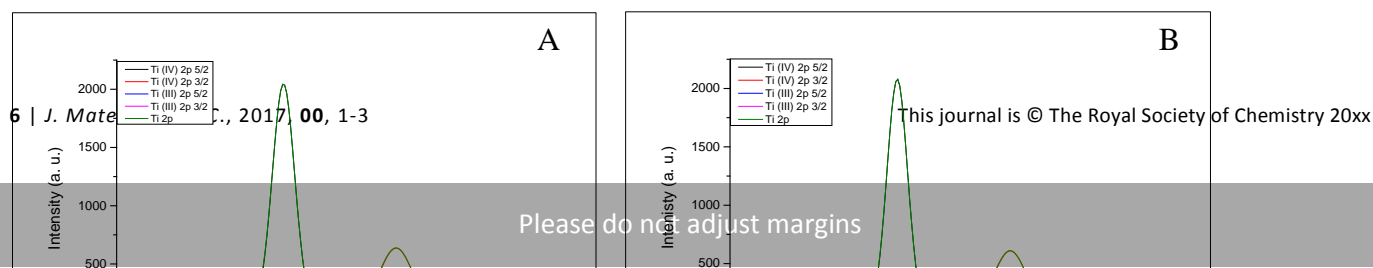


Figure 5 Ti 2p XP spectra of (A) non-doped oleic-acid-stabilised, titanium dioxide (OA-TiO₂) nanorods and the analogous oleic-acid-stabilised, niobium-doped titanium dioxide (OA-Nb-TiO₂) nanorods, prepared from NBEO (B) **S3**, (C) **S4**, (D) **S5** and (E) **S6**.

Table 2: Surface composition and binding energies for Ti (IV), Ti (III), Nb (V) and Nb (IV) ions in the non-doped oleic-acid-stabilised, titanium dioxide (OA-TiO₂) nanorods and the corresponding oleic-acid-stabilised, niobium-doped titanium dioxide (OA-Nb-TiO₂) nanorods **S4-S6**, prepared from NBEO.

Sample	Ti (IV)		Ti (III)		Nb (V)		Nb (IV)	
	B.E. (eV)	Loading (atom%)	B.E. (eV)	Loading (atom%)	B.E. (eV)	Loading (atom%)	B.E. (eV)	Loading (atom%)
OA-TiO ₂	458.35	65.35	456.35	1.33	---	---	---	---
	464.05	32.66	462.05	0.66	---	---	---	---

S3	458.43	64.25	456.44	2.43	206.88	53.02	205.88	7.02
	464.14	32.11	462.14	1.21	209.58	35.29	208.58	4.67
S4	458.43	64.33	456.43	2.35	206.90	53.49	205.88	6.55
	464.13	32.15	462.13	1.17	209.60	35.6	208.58	4.36
S5	458.48	64.68	462.17	3.00	206.88	54.8	205.88	5.24
	464.18	36.86	456.48	1.00	209.58	36.47	208.58	3.49
S6	458.40	54.80	456.40	1.80	206.88	55.38	205.88	4.66
	464.10	36.47	462.10	0.90	209.58	36.86	208.58	3.10

Table 2 Surface composition and binding energies of the non-doped oleic-acid-stabilised, titanium dioxide (OA-TiO₂) nanorods and the corresponding oleic-acid-stabilised, niobium-doped titanium dioxide (OA-Nb-TiO₂) nanorods **S3-S6**.

Sample	O 1s		Ti 2p		C 1s		Nb 3d		N 1s	
	B.E. (eV)	Loading (atom %)	B.E. (eV)	Loading (atom %)	B.E. (eV)	loading (atom %)	B.E. (eV)	loading (atom %)	B.E. (eV)	loading (atom %)
OA-TiO ₂	529.6	27.84	458.4	11.83	284.6	58.5	---	---	398.2	1.82
S3	529.8	30.75	458.5	11.64	284.6	54.89	206.9	1.84	400.8	0.88
S4	529.8	30.15	458.5	10.85	284.6	56.26	207.0	1.74	401.4	1.01
S5	529.7	32.46	458.4	12.26	284.6	52.62	207.0	1.42	339.6	1.23
S6	529.7	29.32	458.4	11.14	284.6	57.34	206.8	0.94	402.0	1.25

$Nb_2O_5 \xrightarrow{2TiO_2} 2Nb_{Ti} + 5O_0 + 2e'$	(10)
$O_0 \leftrightarrow 2e + V_0'' + \frac{1}{2}O_{21}$	(11)
$Ti^{4+} + e \leftrightarrow Ti^{3+}$	(12)

The surface chemical compositions obtained from XPS fitting for the non-doped oleic-acid-stabilised, titanium dioxide (OA-TiO₂) nanorods and the corresponding oleic-acid-stabilised, niobium-doped titanium dioxide (OA-Nb-TiO₂) nanorods **S4-S6**, prepared from NBEO, are shown in Table 3. The atomic ratio of Ti:Nb was 6.32:1 and 6.23:1 (13.7 and 13.8 % Nb) for **S3** and **S4**, respectively, somewhat lower than the bulk loadings determined by ICP of 9.5:1 and 10.2:1 (9.5 and 8.9 % Nb). Similarly, the surface atomic ratio of Ti:Nb was 8.63:1 and 11.85:1 (10.4 and 7.8 % Nb) for **S5** and **S6**, respectively, lower than the bulk ICP values of 13.7:1 and 18.3:1 (6.8 and 5.2 % Nb). These findings suggest a slight segregation of niobium on the surface of the titanium dioxide nanorods. Surface segregation and agglomeration of niobium on titanium dioxide fibres and particles has been reported previously^{30,39} driven by the higher oxygen affinity for niobium than titanium.^{31, 38} The possible reason for the relative low bulk solubility of niobium in titanium oxide is the low reaction temperature (100 °C). Ruiz et al. reported a solubility limit of 10 % niobium into anatase titania,³⁰ but the sample was obtained after heat-treated at 600 °C.

All the oleic-acid-stabilised, niobium-doped titanium dioxide (OA-Nb-TiO₂) nanorods can be readily suspended at

relatively high concentration (10 wt%) in chlorobenzene, as shown in Figure 6 for the nanorods **S3-S6**.

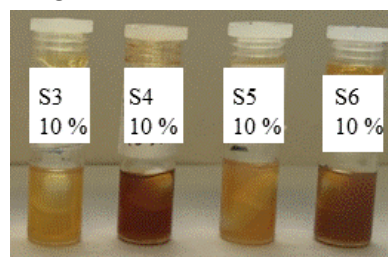


Figure 6 Photographs of the suspensions of oleic-acid-stabilised, niobium-doped titanium dioxide (OA-Nb-TiO₂) nanorods **S3-S6** at relatively high concentration (10 wt%) in chlorobenzene.

Device Performance

The dielectric constant spectra for the oleic-acid-stabilised, niobium-doped (7.12% and 5.6%) titanium dioxide (OA-Nb-TiO₂) nanorods **S4** and **S5**, respectively, and that of the corresponding non-doped, oleic-acid-stabilised, titanium dioxide (OA-TiO₂) nanorods, for comparison purposes, are shown in Figure 7. All spectra indicate a slight increase of the dielectric constant as the frequency is reduced, which is related to polarisation effects involving the device's interface contribution to the impedance.⁴¹ The dielectric constant at frequencies in the region of 100kHz-1MHz is around 6 for the non-doped, oleic-acid-stabilised, titanium dioxide (OA-TiO₂) nanorod reference material, while it increases to more than 8 for the oleic-acid-stabilised, niobium-doped (7.1 wt%) titanium dioxide (OA-Nb-TiO₂) nanorods **S4**. Similarly, current-Voltage leakage current measurements show that an increasing niobium concentration improves the leakage current by reducing it and thereby

preventing hard dielectric breakdown, see Figure 8a. Further analysis of the current-voltage characteristics as shown in Figure 8b, suggests common current-voltage characteristics of the three nanomaterials tested, i.e., a nearly linear behaviour at low voltages (the slight mismatch with a perfectly linear regime could be attributed to the very low current level approaching the detection limit of our instrument), followed by a super-linear behaviour at higher voltages with exponent around 5-6. The former could be attributed to a hopping leakage mechanism⁴², while the latter could indicate a trap-assisted mechanism (power behaviours with such high exponents could be attributable to the Poole-Frenkel mechanism⁴²) although only temperature dependent measurements would allow an in-depth insight in this direction. The major difference between the three trends is the onset voltage of the superlinear regime at ca 3V for the non-doped, oleic-acid-stabilised, titanium dioxide (OA-TiO₂) nanorod reference material, while it increases to more than 10 V for the corresponding oleic-acid-stabilised, niobium-doped (7.1 wt%) titanium dioxide (OA-Nb-TiO₂) nanorods **S4**.

Co-doping of titanium dioxide with donor-acceptor dopants has recently received a lot of interest in terms of the creation of materials with colossal permittivity and low, or improved, loss.⁴³ Niobium is a very common material donor dopant⁴⁴ and niobium doping alone has been reported recently to produce titanium dioxide films with permittivity above 10⁴.⁴⁴ This behaviour could be compatible with the results reported here where niobium doping (7.12%) of the non-doped, oleic-acid-stabilised, titanium dioxide (OA-TiO₂) nanorod reference material increases the dielectric constant by a third (from $k = 6$ to $k > 8$, respectively) for the oleic-acid-stabilised, niobium-doped titanium dioxide (OA-Nb-TiO₂) nanorods **S4**. While such an increase is remarkable for solution-processable dielectric materials, it is probably the presence of a low-dielectric-constant, organic capping of oleic acid around the oleic-acid-stabilised, niobium-doped titanium dioxide (OA-Nb-TiO₂) nanorods **S4** and **S5**, that actually attenuates the high permittivity enhancement achievable with niobium-doping of titanium dioxide, if the low dielectric constant part was absent. Interestingly, niobium doping has also been used in several works as an effective way to increase the conductivity of titanium dioxide electron transporting layers⁴⁵ or to be used just as alternative transparent conductive oxide.⁴⁶

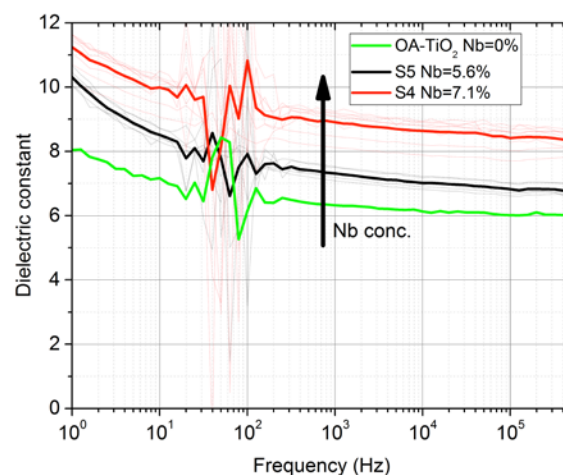
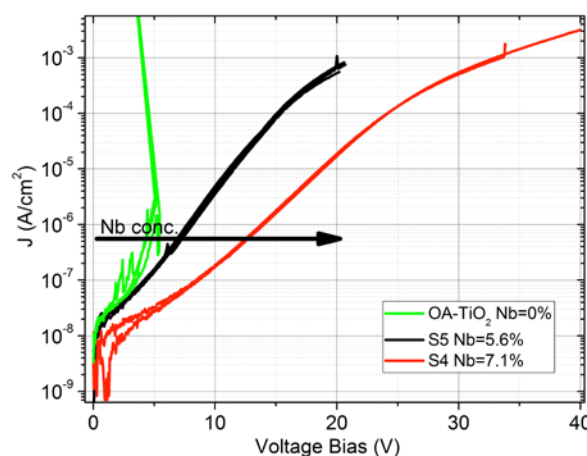
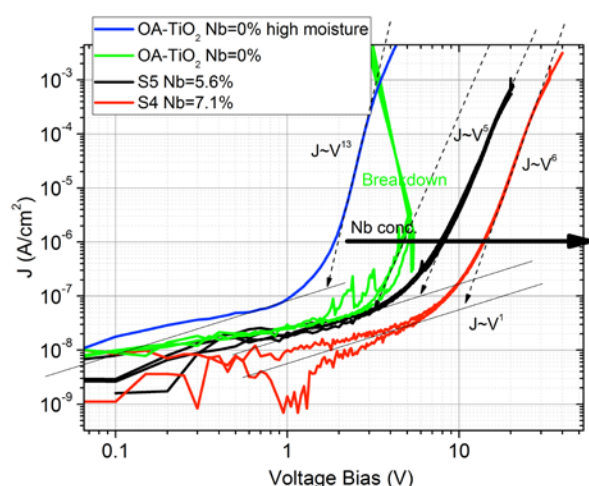


Figure 7 Dielectric constant spectra for the oleic-acid-stabilised, niobium-doped titanium dioxide (OA-Nb-TiO₂) nanorods **S4** and **S5** and that of the corresponding non-doped, oleic-acid-stabilised, titanium dioxide (OA-TiO₂) nanorods, obtained by analysing the impedance data using an R-C parallel model.



(a)



(b)

Figure 8 Current-Voltage Leakage current measurements in inert environment for the oleic-acid-stabilised, niobium-doped titanium dioxide (OA-Nb-TiO₂) nanorods **S4** and **S5** and that of the corresponding non-doped, oleic-acid-stabilised, titanium dioxide (OA-TiO₂) nanorods, a) log-linear plot, b) log-log plot with the high moisture measurement carried out at room temperature and 95% relative humidity in an oxygen-free environment.

Higher levels of niobium doping in the oleic-acid-stabilised, titanium dioxide (OA-Nb-TiO₂) nanorods **S4** and **S5** resulted in improved leakage current of the dielectric film, mainly by increasing the effective onset voltage of the super-linear regime. Electron-pinned defect-dipoles arising from the interaction between niobium and oxygen vacancies create reduced dielectric losses⁴⁴ and could support this interpretation of these results. Moreover, leakage current measurement in an inert nitrogen environment, but the presence of high moisture levels shows that the superlinear regime could actually be related to water, likely adsorbed onto titanium dioxide, as shown by the blue curve in Figure 8b. Thus, it is possible that the observed niobium doping effect on the leakage current could arise from a suppressed water adsorption over the nanorods, due to oxygen vacancy passivation⁴⁷ due to the aforementioned interaction between the niobium dopants and oxygen vacancies.⁴⁴

Conclusions

Novel, low-cost, solution-processable and highly crystalline, niobium-doped titanium dioxide nanorods have been prepared using a one-step hydrolytic condensation reaction. Uniform thin, smooth, and transparent films of these nanorods have been deposited from concentrated solution (10 wt%) in chlorobenzene by spincoating onto standard crossbar test devices. The dielectric constant ($k > 8$ at frequencies in the region of 100 kHz-1 MHz) of these oleic-acid-stabilised,

niobium-doped (7.12%) titanium dioxide (OA-Nb-TiO₂) nanorods is a third higher than that ($k = 6$) of the corresponding non-doped, oleic-acid-stabilised, titanium dioxide (OA-TiO₂) nanorods used as a reference material. Current-Voltage (J - V) leakage current measurements show that a higher niobium concentration improves the leakage current of the test devices by reducing it and preventing hard dielectric breakdown. Electron-pinned defect-dipoles due to electrons and oxygen vacancies located in the limited lattices may be the main reason for the increase of dielectric constant and decrease of dielectric loss in the high frequency range. It is probably the presence of the low-dielectric-constant organic capping of oleic acid around the niobium-doped titanium dioxide (OA-Nb-TiO₂) nanorods that attenuates the high permittivity enhancement.

Conflicts of interest

"There are no conflicts to declare".

Acknowledgements

We thank the EPSRC (EP/J001597/1, EP/K021796/1 and EP/K029525/2) and the King Saud University, Deanship of Scientific Research, College of Science Research Centre for financial support. Mrs A Lowry, Mrs C Kennedy and Dr R Knight are thanked for providing TEM, CHN and ICP analyses, respectively.

Notes and references

- 1 L. Petti, N. Müntenrieder, C. Vogt, H. Faber, L. Büthe, G. Cantarella, F. Bottacchi, T. D. Anthopoulos and G. Tröster, *Appl. Phys. Rev.*, 2016, **3**, 021303 – 021353.
- 2 Y. S. Rim, S. H. Bae, H. Chen, N. D. Marco and Y. Yang, *Adv. Mater.*, 2016, **28**, 4415 – 4440.
- 3 K. R. R. Venkata, A. K. Venkata, P. S. Karthik and S. P. Singh, *RSC Adv.*, 2015, **5**, 77760 – 77790.
- 4 F. Li, B. Shang, P. Ling, L. Wei and Z. Yang, *J. Electron. Mat.*, 2016, **45**, 5178 – 5184.
- 5 B. P. Mandal, P. Anithakumari, S. Nigam and C. Majumder, *New J. Chem.*, 2016, **40**, 9526 – 9536.
- 6 M. R. Beaulieu, J. K. Baral, N. R. Hendricks, Y. Y. Tang, A. L. Briseno and J. J. Watkins, *ACS Appl. Mater. Interfaces*, 2013, **5**, 13096–13103.
- 7 X. Huang and P. K. Jiang, *Adv. Mater.*, 2015, **27**, 546–554.
- 8 S. Faraji, T. Hashimoto, M. L. Turner and I. A. Majewski, *Organic Electronics*, 2015, **17**, 178–183.
- 9 S. Roberts, *Phys. Rev.*, 1949, **76**, 1215 – 1220.
- 10 Z. W. Wang, Q. Li, Z. She, F. Chen and L. Li, *J. Mater. Chem.*, 2012, **22**, 4097 – 4105.
- 11 D. H. Kwon, K. M. Kim, J. H. Jang, J. M. Jeon, M. H. Lee, G. H. Kim, X. S. Li, G. S. Park, B. Lee, S. Han, M. Kim and C. S. Hwang, *Nat. Nanotechnol.*, 2010, **5**, 148 – 153.
- 12 M. Zorn, S. Meuer, N. T. Muhammad, Y. Khalavka, C. S. Tremel, T. Wolfgang and R. Zentel, *J. Mater. Chem.*, 2008, **18**, 3050 – 3058.
- 13 N. R. Jana, *Chem. Commun.*, 2003, 1950 – 1951.
- 14 U. Vukicevic, S. Ziemian (Chyla), A. Bismarck and S. P. Shaffer Milo, *J. Mater. Chem.*, 2008, **18**, 3448 – 3453.
- 15 S. J. Kwon, H. B. Im, J. E. Nam, J. K. Kang and K. B. Hwang Yi, *Appl. Surf. Sci.*, 2014, **320**, 487 – 493.
- 16 B. Santara and P. K. Giri, *Mater. Chem. Phys.*, 2013, **137**, 928 – 936.
- 17 S. Biswas, V. Sundstrom and S. De, *Mater. Chem. Phys.*, 2014, **147**, 761 – 771.
- 18 R. Menzel, B. F. Cottam, S. Ziemian (Chyla) and S. P. Shaffer Milo, *J. Mater. Chem.*, 2012, **22**, 12172 – 12178.
- 19 R. D. Cozzoli, A. Kornowski and H. Weller, *J. Amer. Chem. Soc.*, 2003, **125**, 14539 – 14548.

- 20 Z. Zhang, X. Zhong, S. Liu, D. Li and M. Han, *Angew. Chem Int. Ed. Eng.*, 2005, **117**, 3532 – 3536.
- 21 Sujatha Singh, Harjeet Kaur, V.N. Singh, Kiran Jain and T.D. Senguttuvan, *Sensors and Actuators B*, 2012, **171–172**, 899 – 906.
- 22 B. N. Joshi, H. Yoon, M. F. A. M. van Hest and S. S. Yoon, *J. Am. Ceram. Soc.*, 2013, **96**, 2623–2627
- 23 W. Lee, I. Kim, I. Ok, D. Ahn, H. Lee, J-H Kim and K. Kim, *Thin Solid Films*, 2014, **553**, 161 – 165.
- 24 H. Usui, S. Yoshioka, K. Wasada, M. Shimizu and H. Sakaguchi, *ACS Appl. Mater. Interfaces*, 2015, **7**, 6567 – 6573.
- 25 L. Lu, M. Guo, S. Thornley, X. Han, J. Hu, M. J. Thwaites and G. H. Shao, *Solar Energy Materials & Solar Cells*, 2016, **149**, 310 – 319.
- 26 S. G. Kim, M. J. Ju, I. T. Choi, W. S. Choi, H.-J. Choi, J.-B. Baek and H. K. Kim, *RSC Adv.*, 2013, **3**, 16380 – 16386.
- 27 M. Duta, L. Predoana, J. M. Calderon-Moreno, S. Preda, M. Anastasescu, A. Marin, I. Dascalu, P. Chesler, C. Hornoio, M. Zaharescu, P. Osiceanu and M. Gartner, *Mater. Sci. in Semiconductor Processing*, 2016, **44**, 397 – 404.
- 28 X. Yu, L. Xin, Y. Liu, W. Zhao, B. Li, X. Zhou and H. Shena, *REC Adv.*, 2016, **6**, 27094 – 27101.
- 29 Y. Song, X. Wang, Y. Sui, Z. Liu, H. Zhang, B. Zhan and B. Song, *Scientific Reports*, 2016, **6**, 21478.
- 30 A. M. Ruiz, G. Dezanneau, J. Arbiol, A. Cornet and J. R. Morante, *Chem. Mater.*, 2004, **16**, 862 – 871.
- 31 L. R. Sheppard, T. Dittrich, and M. K. Nowotny, *J. Phys. Chem. C*, 2012, **116**, 20923 – 20929.
- 32 B. K. Kaleji, R. S. Mamoory and A. Fujishim, *Mater. Chem. Phys.*, 2012, **132**, 210 – 215.
- 33 Y. Gao, *Thin Solid Films*, 1999, **346**, 73 – 81.
- 34 Takahashi, R. Takahashi, S. Takenaka, S. Sato, T. Sodesawa, K. Ogura and K. Nakanishi, *J. Chem. Soc., Faraday Trans.*, 1998, **94**, 3161 – 3168.
- 35 M. Nara, H. Torii and M. Tasumi, *J. Phys. Chem.*, 1996, **100**, 19812 – 19817.
- 36 Atashbar, M. Z. Atashbara, H. T. Sun, B. Gong, W. Wlodarski and R. Lam, *Thin Solid Films*, 1998, **326**, 238 – 244.
- 37 W. Hu, Y. Liu, R. L. Withers, T. J. Frankcombe, L. Norén, A. Snashall, M. Kitchin, P. Smith, B. Gong, H. Chen, J. Schiemer, F. Brink and J. W. Leung, *Nature Mater.*, 2013, **12**, 821 – 816.
- 38 M. Fehse, S. Cavaliere, P. E. Lippens, I. Savych, A. Iadecola, L. Monconduit, D. J. Jones, J. Rozière, F. Fischer, C. Tessier and L. Stievano, *J. Phys. Chem. C*, 2013, **117**, 13827 – 13835.
- 39 Ch. Trapalis, V. Kozhukharov and B. Samuneva, *J. Mater. Sci.*, 1993, **28**, 1276 – 1282.
- 40 Z. Gai, Z. Cheng, X. Wang, L. Zhao, N. Yin, R. Abah, M. Zhao, F. Hong, Z. Yu and S. Dou, *J. Mater. Chem. C*, 2014, **2**, 6790 -6795.
- 41 E. Barsoukov and J. R. Macdonald, *Impedance Spectroscopy: Theory, Experiment, and Applications*, Second Edition, Wiley, 2005
- 42 E. Verrelli and D. Tsoukalas, *J. Appl. Phys.*, 2013, **113**, 114103/1 – 114103/8.
- 43 W. Hu, Y. Liu, R. L. Withers, T. J. Frankcombe, L. Norén, A. Snashall, M. Kitchin, P. Smith, B. Gong, H. Chen, J. Schiemer, F. Brink and J. Wong-Leung, *Nature Mater.*, 2013, **12**, 821 – 826.
- 44 F. Li, B. Shang, P. Liang, L. Wei and Z. Yang, *J. Electron. Mater.*, 2016, **45**, 5178 – 5184.
- 45 G. Yin, J. Ma, H. Jiang, J. Li, D. Yang, F. Gao, J. Zeng, Z. Liu and S. F. Liu, *ACS Applied Materials & Interfaces*, 2017, **9**, 10752 – 10758.
- 46 S. Nikodemski, A. A. Dameron, J. D. Perkins, R. P. O'Hayre, D. S. Ginley and J. J. Berry, *Scientific Reports*, 2016, **6**, 32830.
- 47 Y. Zhao, K. Kita, K. Kyuno and A. Toriumi, *Jpn. J. of Appl. Phys. Part 1*, 2007, **46**, 4189 – 4192.